Study of riverine deposits using electromagnetic methods at a low induction number

This is a copy of the paper:
Sambuelli, L., S. Leggieri, C. Calzoni, and C. Porporato. 2007. Study of riverine deposits using electromagnetic methods at a low induction number. Geophysics 72, (5): B113-B120

Study of riverine deposits using electromagnetic methods at low induction number

Journal:	*Geophysics*
Manuscript ID:	GEO-2006-0287.R2
Manuscript Type:	Case History
Date Submitted by the Author:	20-Mar-2007
Complete List of Authors:	Sambuelli, Luigi; Politecnico Di Torino, Dipartimento di Ingegneria del Territorio, dell'Ambiente e delle Geotecnologie Leggieri, Salvatore; Politecnico di Torino, Dipartimento di Ingegneria del Territorio, dell'Ambiente e delle Geotecnologie Calzoni, Corrado; Politecnico di Torino, Dipartimento di Ingegneria del Territorio, dell'Ambiente e delle Geotecnologie Porporato, Chiara; Politecnico di Torino, Dipartimento di Ingegneria del Territorio, dell'Ambiente e delle Geotecnologie
Keywords:	electromagnetics, sediment, mapping
Area of Expertise:	Electrical and Electromagnetic Methods, Engineering and Environmental Geophysics

Study of riverine deposits using electromagnetic methods at low induction number

Luigi Sambuelli*, Salvatore Leggieri, Corrado Calzoni, Chiara Porporato

DITAG – Dipartimento di Ingegneria del Territorio, dell'Ambiente e delle Geotecnologie – Politecnico di Torino – C.so Duca degli Abruzzi, 24 – 10129 – Turin - Italy.

corresponding author: luigi.sambuelli@polito.it

ABSTRACT

We carried out some electromagnetic (EM) profiles along the river Po in the city of Turin (Italy). The aim of this activity was to verify the applicability of low induction number EM multifrequency soundings carried out from a boat in riverine surveys with the intent of determining whether this technique, which is cheaper than air–carried surveys, could be effectively used to define the typology of sediments and to obtain an estimate of the stratigraphy below a riverbed.

We used a GEM-2 (handheld broadband EM sensor) operating with six frequencies to survey the investigated area. A GPR, a conductivity meter and a TDR were used to estimate the bathymetry and to measure the electromagnetic properties of the water. A GPS system, working in RTK mode, was employed to track the route of the boat with centimetric accuracy.

We analyzed the induction number, the depth of investigation (DOI) and the sensitivity of our experimental setup by forward modeling varying the water depth, the frequency and the bottom sediment resistivity. The simulations led to an optimization of the choice of the frequencies that could be reliably used for the interpretation. The 3406 Hz signal had a DOI in the PO water (27 Ωm) of 2.5m and provided sediment resistivities higher than 100 Ωm.

We applied a bathymetric correction to the conductivity data using the water depths obtained from the GPR data. We plotted a map of the river bottom resistivity and compared this map to the results of a direct sediment sampling campaign. The resistivity values (from 120 to 240Ωm) were compatible with the saturated gravel with pebbles in a sandy matrix that resulted from the direct sampling, and with the known geology.

INTRODUCTION

Inland waters can be of great interest from several points of view: civil (i.e., water supplies, waterways, resort activities, material dredging, bridge scours, river bar monitoring, harbor and river engineering), environmental (i.e., interactions with shallow aquifers, recharge areas, erosion, submerged unexploded ordnances (UXO) in bombed industrial cities) or disaster planning (i.e., flood prevention and mitigation). Some usual shallow water geophysics techniques and some other techniques borrowed from near-surface geophysics can help to resolve some of the problems such as, for example, bathymetry mapping, riverbed characterization and UXO detection.

Some experiences referring to boat-carried surveys on inland waters can be found in the literature. Ground penetrating radar (GPR) and seismic methods have been utilized to perform riverine surveys. Beres and Haeni (1991) used GPR to study selected stratified-drift deposits in Connecticut. Dudley and Giffen (2002) ran a GPR survey along 50 miles of the Penobscot River, Maine, in the spring of 1999, to produce maps describing the composition and distribution of streambed sediments. Webb et al. (2000) used a GPR to estimate water depths and identify infilled fluvial scour features, acquired at ten different bridge sites in southeastern and central Missouri. Toth (2004) used a new designed GPR combined with seismic methods to survey the river Danube in the centre of Budapest (Hungary).

The aim of our research was to verify the applicability of an EM dipole-dipole methods with a handheld multi-frequency broadband sensor GEM-2 (Won et al., 1996) to define the typology of the streambed sediments. Up to now, frequency domain electromagnetic systems (FDEM) have been rarely utilized in riverine soundings, also because of electromagnetic interference between the transmitted signal and the boat engine. Butler et al. (2004) carried out a survey concerning these applications to delineate the recharge area to a river valley aquifer on the Saint Joint River (City of Fredericton, New

Brunswick) using a combination of three geophysical surveys: resistivity imaging along the shoreline, seismic and EM methods carried above the water subsurface. The results of the research were successful and the geophysical interpretations were confirmed by drilling.

We acquired GEM-2 multifrequency data on the Po river in Turin (Italy) mainly according to the latter reference (Figure 1).

METHODS

The measurements were conducted along a stretch of the Po River in the city of Turin, near the Valentino park, using the following instruments aboard a motorboat (Figure 2):

- a Geophex GEM-2, handheld broadband conductivity meter;
- a I.D.S. RIS/0 k2, georadar with a TR200 antenna (central frequency 200 MHz);
- a Tektronix 1502c, TDR (Time Domain Reflectometer) to measure water permittivity;
- a ProfiLine-197, conductivity meter to measure water conductivity and temperature;
- two LEICA System 1200 (GPS L1+L2 receivers).

In a first survey, two GPS receivers were placed aboard a boat; one of their antennas was positioned at the stern and the other at the prow of the boat, and both were fixed to the top of a 50 cm wooden pole to assure greater visibility of the antennas and reduce multiple paths. The two receivers were necessary to determine the bearing of the boat and provide a second-by-second geographical reference of the geophysical instruments in an absolute reference system, and to calculate the rotation and translation parameters starting from the knowledge of the antenna positions in both local and global reference systems.

After placing the GPR and the GEM-2 aboard the boat, all the distances between the GPS antennas and the vertices of the geophysical sensors were measured, in order to create a topographic network to position the barycenters of the sensors within a local reference

system that was integral with the boat. During the data processing, the barycentres of the sensors were mapped onto the UTM-WGS84 absolute reference system applying Helmert transformations with seven parameters, that differ for each surveying instant, in order to move all the GPR and GEM-2 measurements, referred to the barycenters of the sensors, from the local to the absolute reference system.

The GPS RTK technique was adopted to define the trajectory and the bearing of the boat in real time and with an accuracy of a few centimeters. Moreover, it was possible to verify the carrier phases initialization directly on field in real time. The stored raw data were also post-processed: in this way, the quality of the positioning was tested and some gaps in the RTK data, due to physical signal obstructions, were filled. The presence of a GPS network is necessary to obtain good results, in terms of accuracy in wide area surveys. This condition also permits the same coherent reference system to be maintained along trajectories of hundreds of kilometers. For the case study, where only a short river stretch was surveyed, the Politecnico di Torino permanent GPS station, which is located almost 2 km away from the surveying area, was used as the RTK master station. A 1 Hz logging rate for the receivers was set up to synchronize the geophysical instruments with the GPS ones. Since the geophysical instrument positioning does not need an accuracy of a few centimeters, it would also be possible to use low-cost single frequency receivers.

We used the GPR for bathymetric estimation in order to test its suitability for deposit characterization in shallow inland waters. We decided to place the GPR antennas aboard the boat instead of on the river bottom because the antenna cable could get caught up in tree-trunks, branches or even in Second World War UXO. The GPR collected, on average, one trace every 3 cm.

The main problem during the GEM-2 data acquisition was the electromagnetic noise produced by the boat engine; to reduce this interference, we positioned the GEM-2 as far as possible from the engine and we used frequencies higher than 500 Hz (according to the

Geophex indications). As we wanted to test the possibility of using a multifrequency broadband sensor to estimate the resistivity of the river bed deposits, during acquisition, we spanned almost the entire GEM-2 frequency range above 500 Hz. The GEM-2 sensor was 0.7 m above the water level and it was set to work using six different frequencies: f_1=775 Hz, f_2=1175 Hz, f_3=3925 Hz, f_4=9825 Hz, f_5=21725 Hz, f_6=47025 Hz. Thus, we obtained six values of apparent resistivity, on average every 0.8 m, theoretically corresponding to six different depths of investigation.

The survey tracks, about 300 m long, are shown in Figure 1. The survey started from the north, near the east riverbank and proceeded southward parallel to the shoreline; a new survey was then carried out along a line parallel to the previous one, but sailing in the opposite direction. On the whole, we acquired 11 tracks (10 parallel to the shoreline and the last zigzagging to transect the river). No information was taken in the areas near the shoreline where the trees prevented the reception of the GPS signal.

After the GPR and GEM-2 acquisition, we used the conductivity meter and the TDR, keeping the boat still in 14 different points (Figure 3) to conduct punctual measurements of the conductivity, temperature and dielectric constant of the water at different depths. In this second survey, the LEIKA GPS allowed us to locate the punctual measurements in points close to the tracks followed in the first survey.

In April 2006, almost five months after the geophysical surveys, the riverbed was sampled utilizing a Van Veen grab bucket. No flood event had occurred in the time that had elapsed from the geophysical survey till the day of the direct sampling survey. Twelve sampling points (Figure 3) were chosen according to the previous geophysical measurements and with the aim of recovering direct information also where the geophysical survey had failed. We were able to position the sampling points with a Garmin GPSMAP 60CS, a GPS system that provided an accuracy of the point locations of about 5 m.

We took 2 or 4 sediment samples for each selected point to obtain an average estimate and to overcome the difficulty of sampling riverbed deposits that were mainly made up of coarse material. However, because of the nature of the deposits, it was impossible to ensure enough material for a complete particle-size analysis.

We also obtained some geological data from a borehole (Figure 1 cross B) drilled about 300 m away on the west bank. This borehole reported "coarse gravel, pebbles, gravel and sand" (Table 1), from 4 m above the level of the river surface to 17 m below it.

DATA PROCESSING

The water conductivity meter and the TDR measurements gave nearly constant water resistivity, temperature and permittivity values. The water resistivity was around 27 Ωm, corresponding to a mean conductivity value of 37 mS/m; the temperature was around 13 °C and the relative permittivity was about 84. Table 2 reports the values measured at the first and last measurement points, the mean value and the standard deviation on the whole set of points.

We processed the GPR raw data utilizing the "Reflex-Win" software. This allowed us to estimate the water depth at each measurement point by picking the time of the bottom reflections at each trace and using the conductivity and permittivity data to calculate the radar pulse velocity. The GPR reflected signals were in a band centered at 200 MHz, corresponding to a wavelength of about 16 cm and gave a depth resolution of about 5 cm. The bathymetric map in Figure 3 shows that the depth of the riverbed increases from the east going toward the west riverbank.

We downloaded the raw data logged by the GEM-2 using the "WinGEM" software, obtaining an apparent conductivity profile (mS/m) for each frequency along each survey track. The raw data power spectra, on average, showed a decrease in energy content below $\lambda \cong 15$ m. The profiles were then low-pass zero-phase filtered (Band-pass filter gain: ≥ -1dB

@λ≥15m; Reject-band filter gain: –100dB@λ≤6.5m) in order to remove the highest spatial frequencies (Figure 4). This processing was necessary because of the high environmental noise which increased with the lowering of the frequency (Figure 5).

The DOI of a handheld conductivity meter depends on many factors: sensor sensitivity, precision, operating frequencies, ambient noise level, target and host properties and intercoil distance. According to Huang (2005), we carried out an analysis to assess: a) the conditions of low induction number, in order to check which frequencies gave a quadrature response that could be converted into conductivity data; b) the capability of the selected frequencies to reliably detect the river bottom sediment, that is, the DOI; c) the capability to reliably discriminate among sediments having different resistivity, that is, the sensitivity.

For this purpose, we conducted a set of simulations that spanned a 500 Hz to 50 kHz frequency range with 6 frequencies per decade, a water resistivity of 27 Ωm, a 1 to 3 m water depth range and a 13.5 to 532 Ωm sediment resistivity range. These latter two ranges were selected on the basis of the bathymetric and the geological data. We carried out this analysis using the Anderson modeling software (1979). We obtained 25 synthetic apparent conductivities (corresponding to five depths in the 1 to 3 m range, as well as 5 resistivity values in the 13.5 to 532 Ωm range) using this simulation at each of the following frequencies: 733.9 Hz, 1077.22 Hz, 3406 Hz, 10772.2 Hz, 23208 Hz and 50000 Hz. We used these results to make comparison with experimental data respectively at 775 Hz, 1175 Hz, 3925Hz, 9825 Hz, 21725 Hz and 47025 Hz.

The apparent conductivity can only be calculated from the quadrature response of the conductivity meter when it operates at an induction number much lower than 1 (Mc Neill, 1980). Moreover, Huang and Won (2003) demonstrated that the induction number has to be larger then 0.02, otherwise the EM response is small and has a small dependence on the

frequency. Therefore, it is possible to only consider reliable those electromagnetic responses that are obtained when the induction number is included in the following range:

$$0.02 < B = \frac{s}{\delta} = \sqrt{\frac{i\omega\sigma\mu_0}{2}}s << 1. \quad (1)$$

Given the GEM-2 inter-coil spacing ($s = 1.66$ m) and the magnetic permeability of free space ($\mu_0=4\pi\times10^{-7}$ H/m), we calculated the mean and standard deviation of the induction numbers relative to the conductivities obtained from the simulation. The results are shown in the plot of Figure 6. We can observe that only the frequencies in the 3 to 22 kHz range produce reliable induction numbers in the 0.02 to 0.085 range (justification of this upper limit is given in Appendix A). We were then only able to obtain reliable conductivity values from the 3406 Hz, 10772 Hz and 23208 Hz signals.

We then estimated the DOI relative to these three frequencies, with the results of the simulations, for different water depths and sediment resistivities, according to the criterion given by Huang (2005). The results of each frequency are plotted in the graphs of Figure 7. Each of these three graphs plots the ratio of the apparent conductivity of a water layer over sediments (σ_a) to the apparent conductivity of an indefinite water layer (σ_{aw}) versus the ratio of the sediment resistivity (ρ_s) to the water resistivity (ρ_w). The two horizontal lines represent the 20% thresholds and the curved lines represent (σ_a/σ_{aw}) at five different water depths. According to the results of these simulations, if we accept a threshold value of 20% - that is, we can detect a sediment if the measured apparent conductivity differs by more than 20% from the apparent conductivity one would have measured above water alone ($\sigma_a/\sigma_{aw}=1$) - the following considerations can be drawn concerning the sensitivity and the DOI.

All the graphs show that there is quite a low sensitivity to the resistivity of the sediments, particularly if the sediments are more resistive than the water (the curves have a

very weak slope when $\rho_s > \rho_w$) and that the sensitivity grows as the frequency and the riverbed depth decreases.

We were only able to obtain a very rough capability to discriminate between coarse (>100 Ωm) and finer (<100 Ωm) sediments from the 3406 Hz signal down to a depth of 2.5 m; when the water depth was lower than 1.5 m we were also able to discriminate between sediments with different resistivities. We were only able to obtain a very rough capability to discriminate between coarse (>100 Ωm) and finer (<100 Ωm) sediments from the 10772 Hz signal down to a depth of 2 m; when the water depth was lower than 1 m we were also able to discriminate between sediments with different resistivities. We were only able to obtain a very rough capability to discriminate between coarse (>100 Ωm) and finer (<100 Ωm) sediments from the highest frequency (23208 Hz) down to a depth of 1 m, which was the minimum water depth we encountered in the survey. This means that the information carried by this latter signal is mainly relative to the bathymetry.

Finally, the results of the simulations showed that information on sediment resistivity could be drawn, from the 3406 Hz signals, only if both the water depth is lower than 2.5 m and the sediment resistivity is higher than 100 Ωm and, from the 10772 Hz signals, only if both the water depth is lower than 2.0 m and the sediment resistivity is higher than 100 Ωm. In order to analyze a larger area and more reliable data, we only focused attention on the 3925 Hz experimental data.

As suggested by Butler et al. (2004), we then made an approximate bathymetric correction on the whole investigated area. We hypothesized a two-layer model (water-sediment) to estimate the sediment resistivity. The apparent conductivity σ_a of a two-layer model is (McNeill, 1980):

$$\sigma_a = \sigma_1\left[1 - R_v(Z)\right] + \sigma_2 R_v(Z) \qquad (2)$$

where $Z=z/s$ is the actual depth divided by the inter-coil spacing s and $R_v(Z)$:

$$R_v(Z) = \frac{1}{\sqrt{4Z^2 + 1}} \tag{3}$$

is the cumulative response of the mathematical function $S_v(Z)$:

$$S_v(Z) = \frac{4Z}{\sqrt{(4Z^2 + 1)^3}} \tag{4}$$

which describes, for vertical magnetic dipole setting, the relative contribution to the secondary magnetic field, measured at the surface, due to a thin horizontal layer at any given depth z.

Since both GPR and GEM2 measurements were referenced in the UTM-WGS84 absolute coordinate system, it was possible to pair each point where apparent conductivity was measured with the respective water depth z_w and to calculate $Z_w = z_w/s$. As reported above, we measured the true water conductivity with the conductivity meter and obtained an average value σ_w = 37 mS/m. Then, we calculated the conductivity of the second layer, which corresponds to the conductivity of the bottom sediment (σ_{sed}) considered as a semi-infinite space at each point of the survey:

$$\sigma_{sed} = \frac{\sigma_a - [1 - R_v(Z_w)]\sigma_w}{R_v(Z_w)} \tag{5}$$

The effect of the water layer was removed through the application of the bathymetric correction.

RESULTS

We plotted a map (Figure 8) of the sediment resistivity at 3925 Hz, discarding the data deeper than 2.5 m and with resistivity lower than 100 Ωm. The most frequent resistivity value was 120 Ωm and 75% of the resistivity values were between 100 and 240 Ωm. These data suggest quite a large homogeneity of the deposits, which mainly consist of saturated gravel with pebbles in a sandy matrix; the latter can be prevalent in a lower resistivity area.

As shown in Table 3, the top of the riverbed in the surveyed area consists of pebbles and coarse gravel alluviums in a sandy-silty matrix (Figure 9). From a careful observation of the samples, it emerges that the alluviums are usually covered by a thin blackish silt film (approximately 1-2 cm), which is rich in organic matter. In the presence of a thicker silt film, it would have been possible to sample a larger amount of sediment but, in our specific case, the grab bucket only managed to scrape off part of the pebbly bottom and pull out huge clasts, in such a way that the finer fraction was very likely to have been underestimated. It is also important to underline that the pebbles had an imbricate structure. This structure did not permit the grab bucket to penetrate, unless one of the two jaws managed to get underneath a pebble. Moreover, even when this happened, the jaws were not able to close completely; therefore the finer material was likely washed away.

Pebbly layers occur during floods, when the water speed is high enough to shift coarse clasts along a riverbed. After a flood, during a low water regime, it is possible to observe the deposit of fine suspended sediments in the areas of a river where there is a decrease in the flow-rate compared to the upstream flow-rate. Similar phenomena occur in natural river beds as hollows, meander scars connected to secondary branches or behind obstacles.

A comparison between the sampling description and the average sediment resistivity around the sampling points is shown in Table 3. The average resistivity values were obtained from the 3925 Hz map. We averaged the resistivities of the 8 points around the sampling points with the resistivity corresponding to the sampling points.

CONCLUSIONS

The sampling of the riverbed sediment only partially confirmed the interpretation of the GEM-2 data filtered and corrected for the bathymetry. We found resistivity values that

were compatible with the average results of the direct sampling and with the known geology, but some sampling results did not agree with the resistivity values obtained in the same point. These discrepancies could be due to the following factors: the difficulty in sampling a significant quantity of depositional material due to the heterogeneous and large dimension of the clasts in comparison to the bucket dimensions; a coarser boat location during the direct sampling due to the lower accuracy of the GPS system used in the direct sampling and to the drift of the boat.

The proposed method, however, if carefully planned and if the results are properly processed, seems to be an effective way of estimating river bed conductivity. We conducted a sensitivity analysis, as part of the data processing, to set reliability limits for our results, concerning the frequency, the resistivity range and the depth of investigation. We also proposed a simple method, with a criterion driven by the error accepted in the approximation, to set the upper limit of the low induction number condition. The analysis we carried out should, as far as possible, always be made when designing and processing surveys of this type, according to the adopted inter-coil distances and frequencies.

The EM modeling highlighted a low sensitivity of the method to the sediment resistivity, especially when this is greater than the water resistivity. This effect also prevented a clear correlation between direct sampling and sediment resistivity.

It could be of interest to test this technique in sites where it is possible to find also finer deposits, especially near a main inlet of an artificial or natural lake or where a horizontal variation of the river bed deposits occurs at a decameter scale.

Improvements could also be obtained moving the sensor away from the boat engine which could result in a better signal-to-noise ratio but also in a larger spread-out of the equipment and in a more difficult positioning.

The GPS measurements were very useful, as they assured smooth comparisons and overlaps between the GEM-2 and GPR responses, which was crucial to perform the

bathymetric correction. Furthermore, the RTK mode made it possible to obtain knowledge on the coordinates with centimetric accuracy in real time, allowing the location of punctual measurements, taken with the conductivity meter, near the tracks followed during the continuous measurements (GPR e GEM-2).

ACKNOWLEDGEMENTS

The authors wish to thank the "Reale Società Canottieri Cerea" of Turin for supplying the boat and the steersman, Professor Alberto Godio for the TDR measurements and fruitful discussions, Eng. Stefano Stocco for the conductivity meter measurements, Eng. Emanuele Pesenti for the help in the GPS operations and Hydrodata S.p.A. for the sampling of the bottom sediments. The authors also wish to thank the reviewers whose observations have greatly improved the manuscript.

APPENDIX A – JUSTIFICATION OF THE SELECTED UPPER LIMIT OF THE LOW INDUCTION NUMBER CONDITION.

As far as the definition of the upper limit of the low induction number condition expressed in eq.1 is concerned, we worked as follows. We calculated, using the six frequencies (775, 1175, 3925, 9825, 21725 and 47025 Hz) used in the survey, over 21 half spaces with different conductivities (from 0.0037 to 0.104 S/m in steps of 0.005 S/m), the response and the induction number for two horizontal 1.66 m distant coils. We made the calculations of the response with both the simplified form $\left(\frac{H_s}{H_p}\right)_{V^S}$ and the "complete" form $\left(\frac{H_s}{H_p}\right)_{V^C}$ (McNeill, 1980).

The complete form is:

$$\left(\frac{H_s}{H_p}\right)_{V^C} = \frac{2}{(\gamma \cdot s)^2}\left\{9 - \left[9 + 9\cdot\gamma\cdot s + 4\cdot(\gamma\cdot s)^2 + (\gamma\cdot s)^3\right]e^{-(\gamma\cdot s)}\right\} \qquad \text{A-1}$$

where:

$\gamma = \sqrt{i \cdot \omega \cdot \mu_0 \cdot \sigma}$

$\omega = 2\pi \cdot f$

$f =$ frequency

$\mu_0 =$ free space permeability $\left[4\pi \times 10^{-7}\right]$

$\sigma =$ half space conductivity

$s =$ inter-coil distance

$i = \sqrt{-1}$

The simplified form is:

$$\left(\frac{H_s}{H_p}\right)_{V^S} = \frac{i \cdot \omega \cdot \mu_0 \cdot \sigma \cdot s^2}{4} \qquad \text{A-2}$$

The induction number is:

$$B = \frac{\sqrt{i \cdot \omega \cdot \mu_0 \cdot \sigma} \cdot s}{\sqrt{2}} \qquad \text{A-3}$$

We then defined a normalized per-cent difference *npd* between the imaginary parts of the simplified and the complete form as:

$$npd = \left\{\left[\mathrm{Im}\left(\frac{H_s}{H_p}\right)_{V^S} - \mathrm{Im}\left(\frac{H_s}{H_p}\right)_{V^C}\right] \Big/ \mathrm{Im}\left(\frac{H_s}{H_p}\right)_{V^C}\right\} \times 100 \qquad \text{A-4}$$

we plotted the *npd* versus B and obtained the graph shown in Figure A-1.

We chose an npd value equal to 10% and obtained an upper limit of B equal to 0.085.

REFERENCES

Anderson, W. L., 1979, Numerical integration of related Hankel transforms of orders 0 and 1 by adaptive digital filtering, Geophysics, **44**, 1287-1305.

Beres, M. and F. P. Haeni, 1991, Application of ground-penetrating-radar methods in hydrogeologic studies, Ground water, **29**, 375–386.

Butler, K. E., J. C. Nadeau, R. Parrott and A. Daigle, 2004, Delineating recharge to a river valley aquifer by riverine seismic and EM methods, Journal of Environmental & Engineering Geophysics, **9**, 95–109.

Dudley, R. W. and S.E. Giffen, 1999, Composition and distribution of streambed sediments in the Penobscot river, Maine, U.S.G.S Water-Resources Investigations Report 01-4223.

Huang, H. and I. J. Won, 2003, Real-time resistivity sounding using a hand-held broadband electromagnetic sensor, Geophysics, **68**, 1224–1231.

Huang, H., 2005, Depth of investigation for small broadband electromagnetic sensor, Geophysics, **70**, 135–142.

McNeill J. D., 1980, Electromagnetic terrain conductivity measurement at low induction numbers, Technical Note TN-6, Geonics Limited.

Toth, T., 2004, High resolution geophysics provides optimal results on inland waterways, First break, **22**, SEP, 45-51.

Webb, D. J., N. L. Anderson, T. Newton and S. Cardimona, 2000, Bridge Scour: Application of ground penetrating radar, MoDOT special publication.

Won, I. J., D. Keiswetter, G. Fields, and L. Sutton, 1996, GEM-2: a new multifrequency electromagnetic sensor , Journal of Environmental & Engineering Geophysics, **1**, 129–137.

CAPTION OF FIGURES

Figure 1 – Localization of the investigated area with the survey tracks: the white lines indicate the continuous measurements (GEM-2 and GPR); the white cross in the NW corner of the map indicates the borehole (B) location.

Figure 2 – Layout of the motorboat used for the survey: A_1 and A_2 are the DGPS antennas; the dimensions are in meters.

Figure 3 - Bathymetric map derived from GPR data: the triangles (P1-P14) refer to the water conductivity and permittivity sampling points; the circles (1-12) refer to river bottom sampling points.

Figure 4 - Power spectrum (above) and conductivity profile (below). Comparison between raw (dashed line) and filtered (continuous line) data for track 3 at 3925 Hz (the third track from the West bank).

Figure 5 – Raw conductivity profiles relative to all frequencies along track 3.

Figure 6 - Mean and standard deviation plot graph of the induction numbers estimated from the modeling in the 500-50000 Hz frequency range. Modeling was made assuming: water resistivity 27 Ωm; sediment resistivity from 13.5 to 532 Ωm; water depth from 1 to 3m; inter-coil distance 1.66 m; sensor height above the water 0.7 m.

Figure 7 – Synthetic apparent conductivity curves (normalized to the apparent conductivity of a water half-space) as a function of sediment resistivity (normalized to water resistivity). The horizontal dashed lines at 0.8 and 1.2 are the DOI thresholds. The parts of the curves outside this interval indicate detectable sediment resistivities. The slope of the curves refers to the sensitivity. The analyzed frequencies were: a) 3406 Hz, b) 10772 Hz and c) 23208 Hz. Modeling was made assuming: water resistivity 27 Ωm; sediment resistivity from 13.5 to 532 Ωm; water depth from 1 to 3m; inter-coil distance 1.66 m; sensor height above the water 0.7 m.

Figure 8 – Resistivity map at 3925 Hz, after bathymetry correction. The circles (1-12) refer to the river bottom sampling points. Only points with a water depth of less than 2.5 m were considered.

Figure 9 – Example of coarse riverbed sampled material.

Figure A-1: Graph relating the normalized per-cent difference (npd) between the simplified form and the complete form of the quadrature component. The dashed band represents the B value range ($0.02 < B < 0.085$) that was considered. The upper B limit was obtained, as indicated by the black arrows, considering the largest acceptable npd equal to 10%.

TABLES

Table. 1 – Borehole B stratigraphy (see Figure 1 for the borehole location)

DEPTH [m]	GEOLOGY
0 ÷ 1,00	Top soil
1,00 ÷ 4,00	Sand, gravel and pebbles
4,00 ÷ 6,00	Coarse sand
6,00 ÷ 11,00	Gravel and large pebbles
11,00 ÷ 13,00	Hard 30- 40 cm thick conglomerates, alternated with loose gravel
13,00 ÷ 13,50	Coarse gravel
13,50 ÷ 15,00	Gravel and large pebbles
15,00 ÷ 16,00	Gravel
16,00 ÷ 17,00	Sand and gravel
17,00 ÷ 23,00	Coarse sand and gravel, water table at 17 m (Po water level)
23,00 ÷ 25,00	Gravel and semi -cohesive sand
25,00 ÷ 26,50	Gravel and loose sand
26,50 ÷ 28,00	Gravel
28,00 ÷ 33,50	Gravel and pebbles (lower part of the Holocene alluvium) transgressive over the Miocene
33,50 ÷ 63,00	Grey compact clayey marl
63,00 ÷ 67,00	Hard marl with scarce pebbles

Table 2 – Conductivity, temperature and permittivity measurements: first point (P1), last point (P14), mean and standard deviation values of 14 points.

	P1			P14			Mean values (14 pts.)			Standard deviations (14 pts.)		
Depth (m)	Conduc. (mS/m)	Temp (°C)	Permittivity [-]	Conduc. (mS/m)	Temp (°C)	Permittivity [-]	Conduc. (mS/m)	Temp (°C)	Permittivity [-]	Conduc. (mS/m)	Temp (°C)	Permittivity [-]
0	39.1	13.7	89	36.7	13.3	81	36.8	13.3	85	0.62	0.12	3
0.5	38.5	13.3	90	36.7	13.3	81	36.8	13.3	84	0.47	0.06	3
1	38.3	13.2	90	36.7	13.3	83	36.7	13.3	85	0.43	0.06	3
1.5	38.2	13.2	88	36.7	13.3	81	36.8	13.3	83	0.41	0.06	3
2	-	-	-	36.7	13.3	-	-	13.3	-	-	0.07	-

Table 3- Riverbed sampling results at each point with the corresponding average resistivities. Each average resistivity was obtained from the 3925 Hz map by averaging the resistivity read at the coordinate of the sampling point with the resistivities of the 8 closest points.

Sampling Points	East UTM-WGS84	North UTM-WGS84	Sample description	Max. clast diameter [cm]	Average resistivity [Ωm]
1	396705	4989732	4 coarse clasts with a small amount of sandy silt	6	180
2	396708	4989729	4 coarse clasts with a little amount of sandy silt	6	215
3	396720	4989751	3 coarse clasts in gravel matrix with silty sand	9	180
4	396714	4989720	1 coarse clast in silt and gravel matrix	7	175
5	396692	4989652	Silt with sandy gravel	<1	225
6	396686	4989643	3 coarse clasts with sandy-silty gravel	8	160
7	396671	4989609	1 coarse clast in sandy-gravelly silt	7	180
8	396761	4989837	2 coarse clasts with sandy-silty pit-run gravel	10	175
9	396624	4989621	1 coarse clast covered by silt	9	-
10	396630	4989637	2 coarse clasts with pit-run gravel (relatively abundant)	8	-
11	396649	4989674	Gravel with sand	<1	-
12	396615	4989578	2 coarse clasts in gravelly-silty sand matrix	6	-

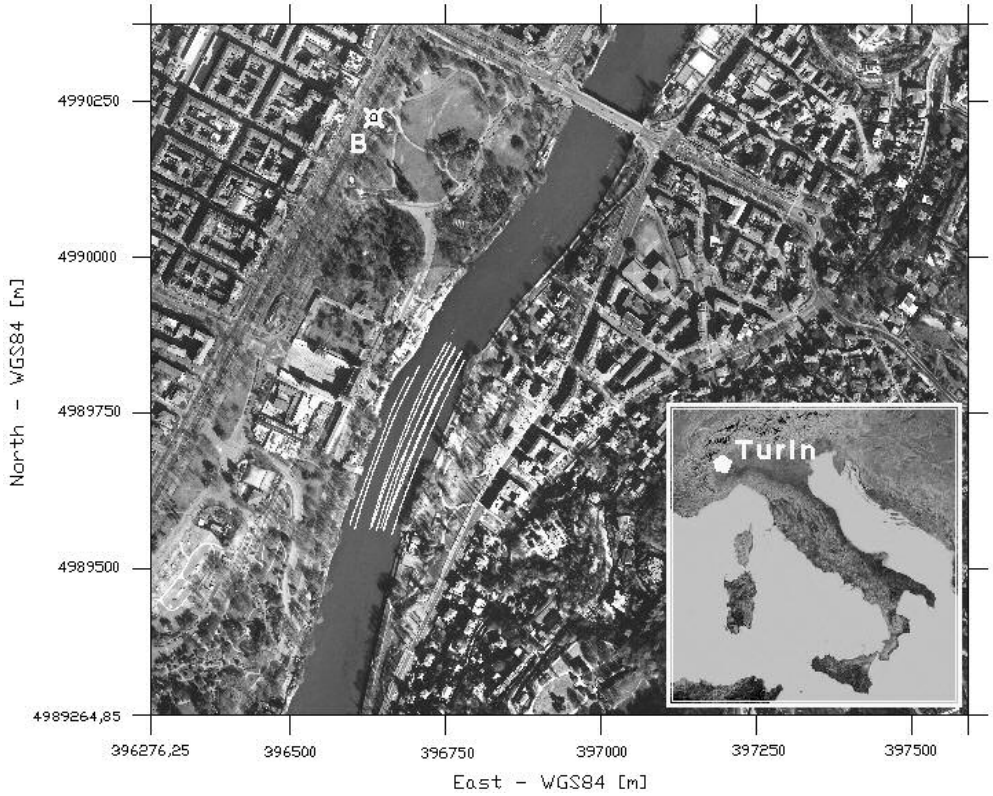

Figure 1 □ Localization of the investigated area with the survey tracks: the white lines indicate the continuous measurements (GEM-2 and GPR); the white cross in the NW corner of the map indicates the borehole (B) location.

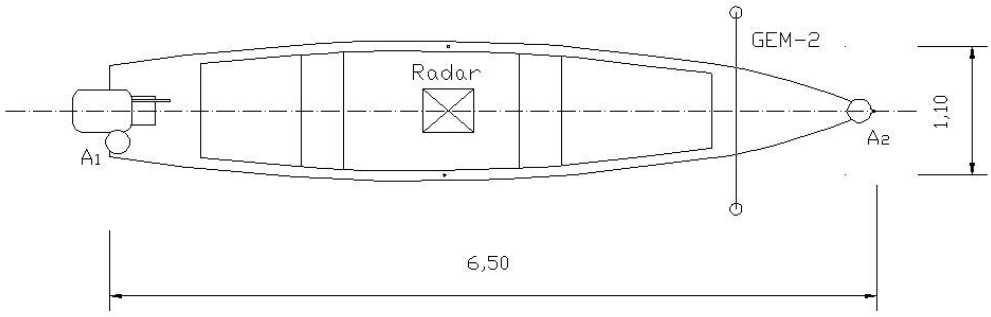

Figure 2 □ Layout of the motorboat used for the survey: A1 and A2 are the DGPS antennas; the dimensions are in meters.

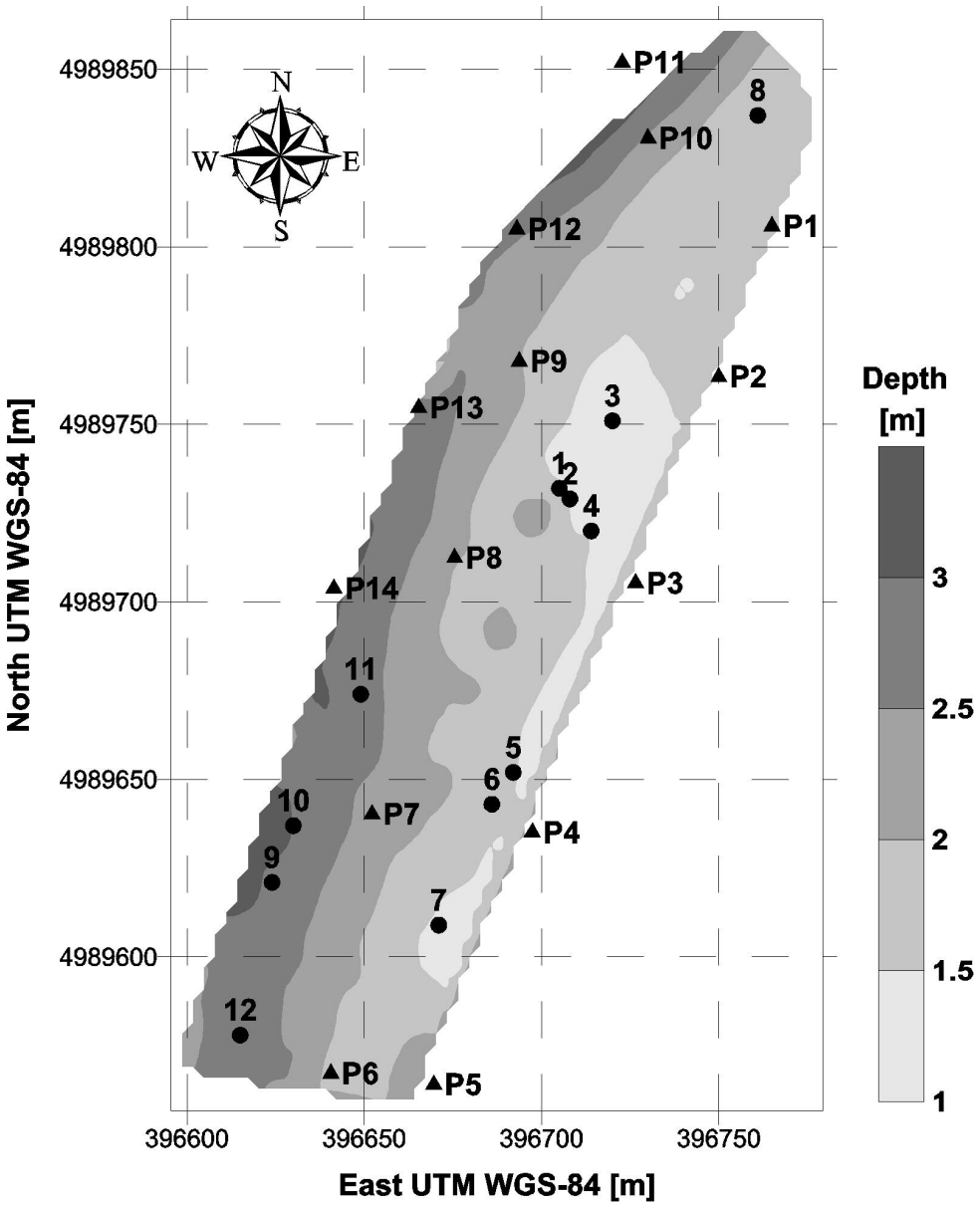

Figure 3 - Bathymetric map derived from GPR data: the triangles (P1-P14) refer to the water conductivity and permittivity sampling points; the circles (1-12) refer to river bottom sampling points.

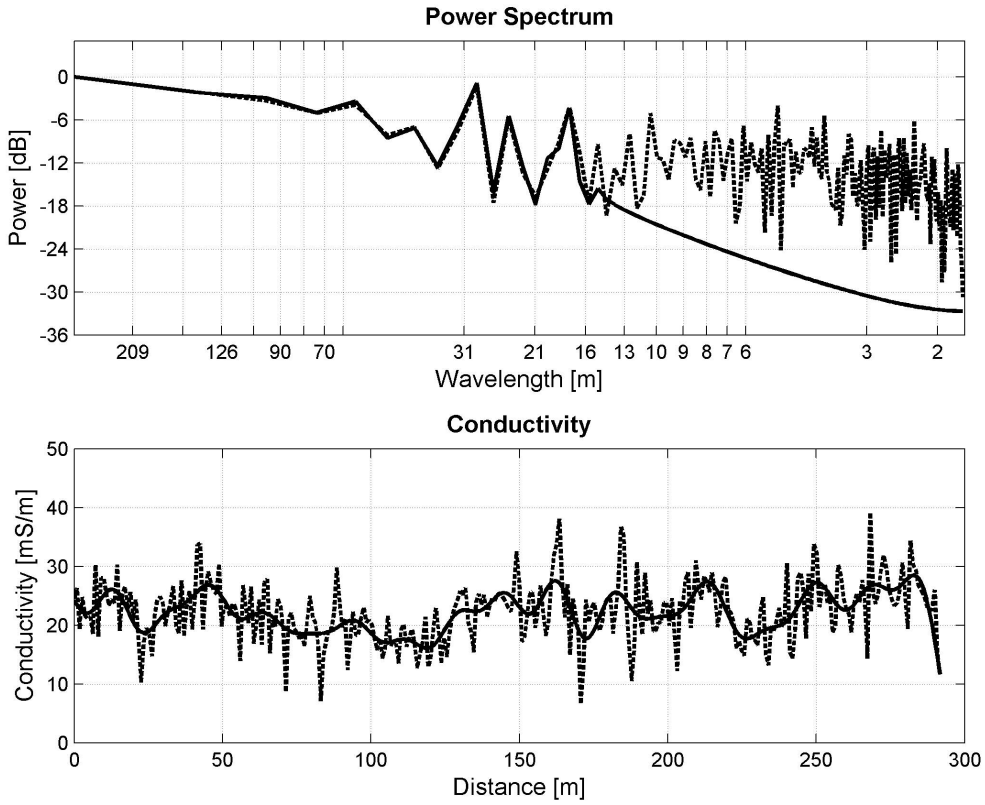

Figure 4 - Power spectrum (above) and conductivity profile (below). Comparison between raw (dashed line) and filtered (continuous line) data for track 3 at 3925 Hz (the third track from the West bank).

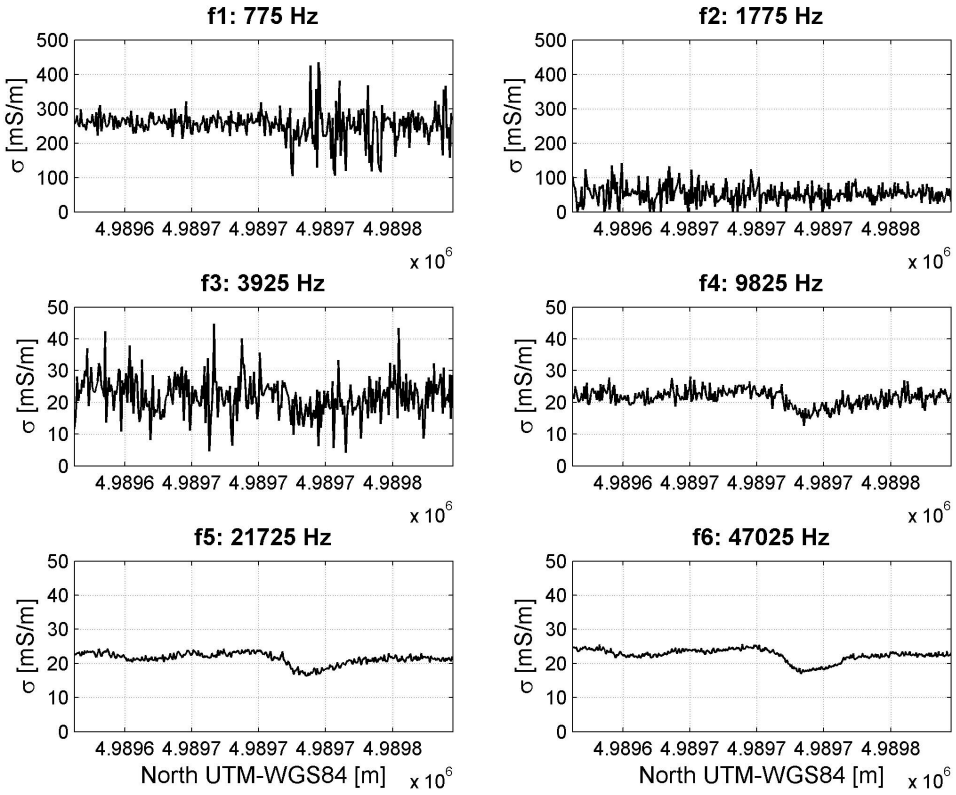

Figure 5 ☐ Raw conductivity profiles relative to all frequencies along track 3.

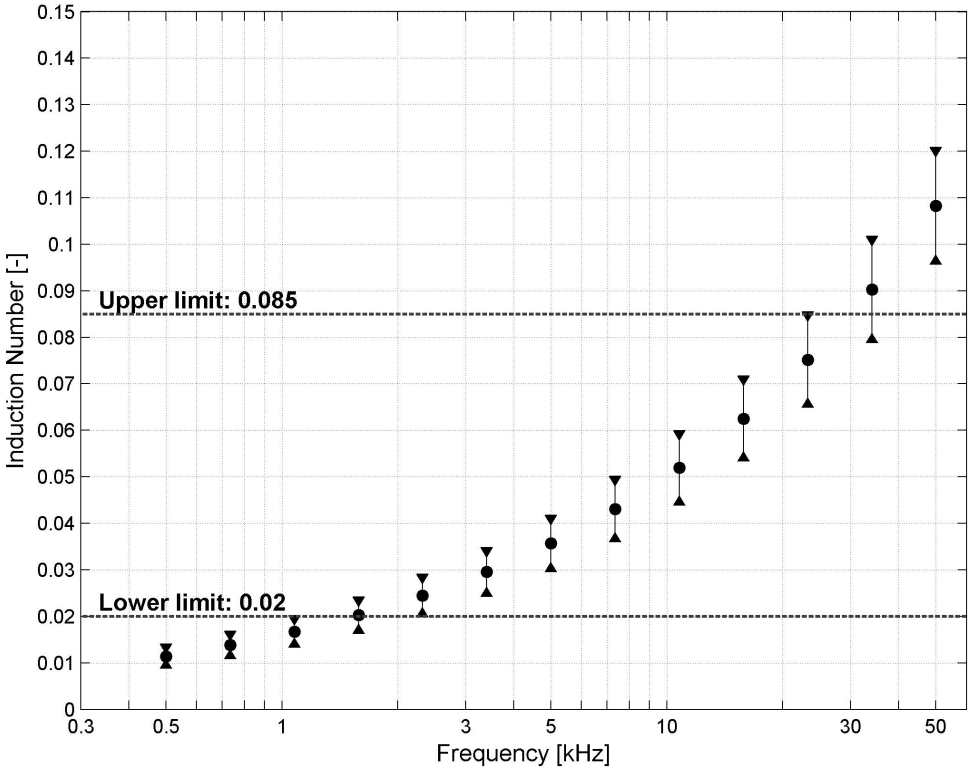

Figure 6 - Mean and standard deviation plot graph of the induction numbers estimated from the modeling in the 500-50000 Hz frequency range. Modeling was made assuming: water resistivity 27 Ωm; sediment resistivity from 13.5 to 532 Ωm; water depth from 1 to 3m; inter-coil distance 1.66 m; sensor height above the water 0.7 m.

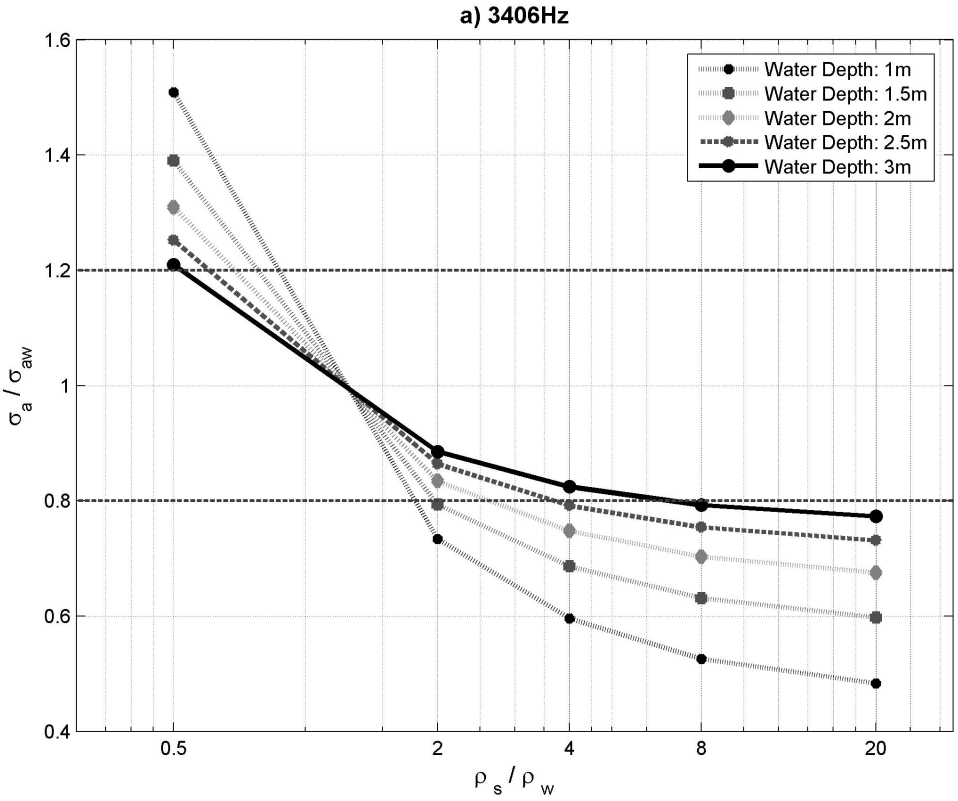

Figure 7 □ Synthetic apparent conductivity curves (normalized to the apparent conductivity of a water half-space) as a function of sediment resistivity (normalized to water resistivity). The horizontal dashed lines at 0.8 and 1.2 are the DOI thresholds. The parts of the curves outside this interval indicate detectable sediment resistivities. The slope of the curves refers to the sensitivity. The analyzed frequencies were: a) 3406 Hz, b) 10772 Hz and c) 23208 Hz. Modeling was made assuming: water resistivity 27 Ωm; sediment resistivity from 13.5 to 532 Ωm; water depth from 1 to 3m; inter-coil distance 1.66 m; sensor height above the water 0.7 m.

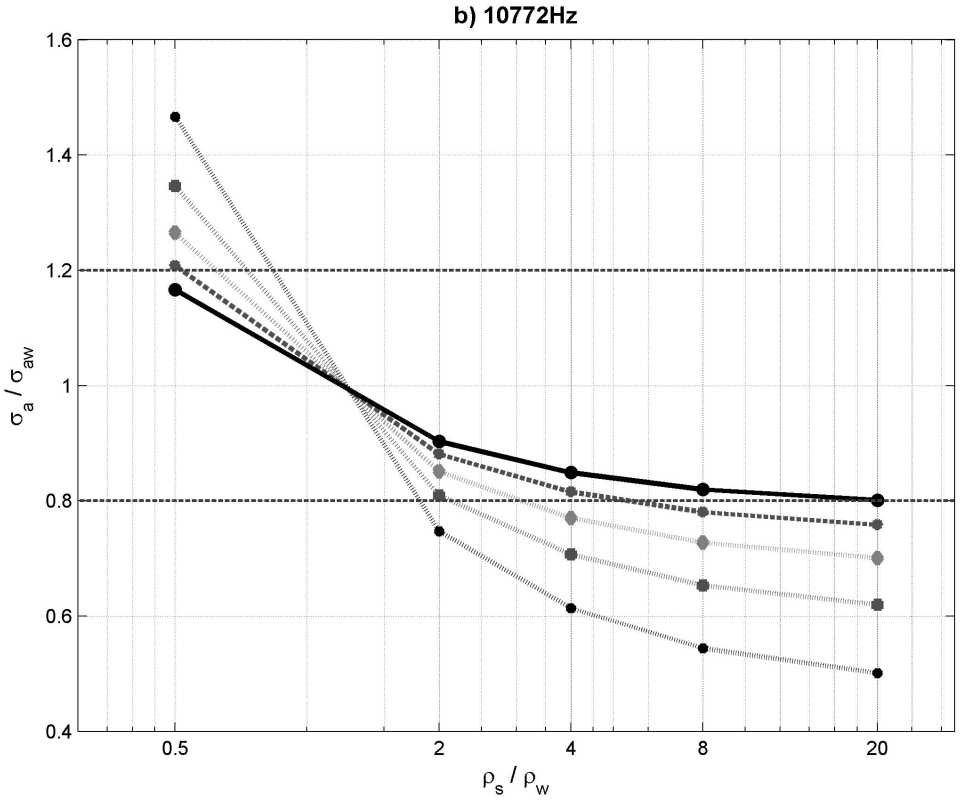

Figure 7 □ Synthetic apparent conductivity curves (normalized to the apparent conductivity of a water half-space) as a function of sediment resistivity (normalized to water resistivity). The horizontal dashed lines at 0.8 and 1.2 are the DOI thresholds. The parts of the curves outside this interval indicate detectable sediment resistivities. The slope of the curves refers to the sensitivity. The analyzed frequencies were: a) 3406 Hz, b) 10772 Hz and c) 23208 Hz. Modeling was made assuming: water resistivity 27 Ωm; sediment resistivity from 13.5 to 532 Ωm; water depth from 1 to 3m; inter-coil distance 1.66 m; sensor height above the water 0.7 m.

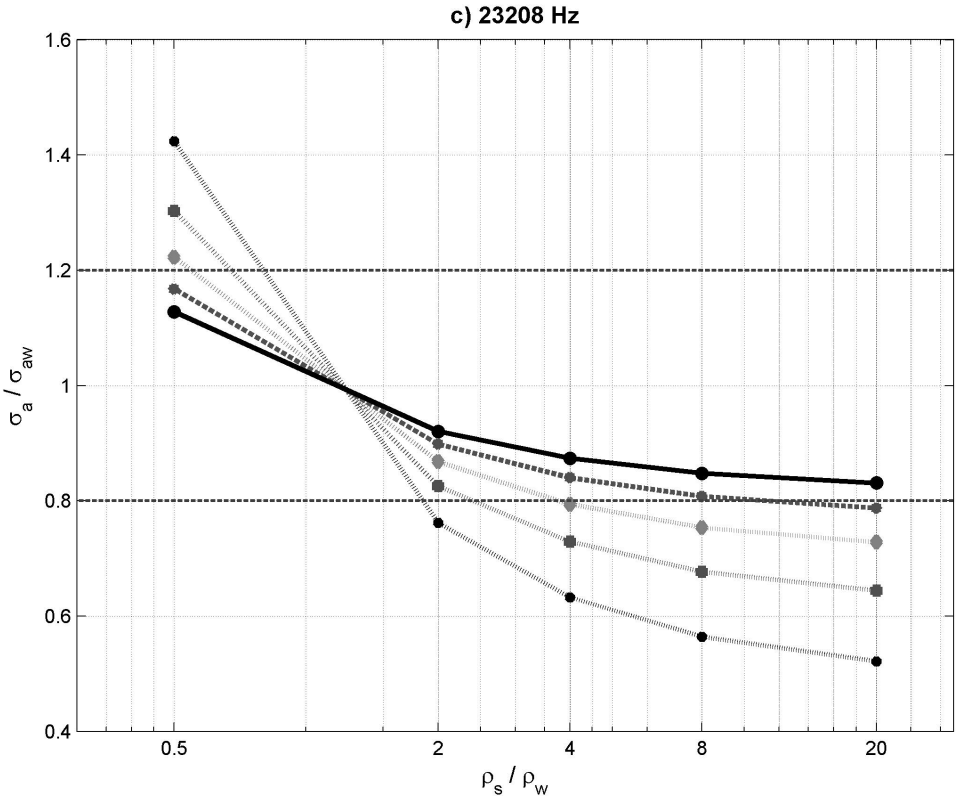

Figure 7 □ Synthetic apparent conductivity curves (normalized to the apparent conductivity of a water half-space) as a function of sediment resistivity (normalized to water resistivity). The horizontal dashed lines at 0.8 and 1.2 are the DOI thresholds. The parts of the curves outside this interval indicate detectable sediment resistivities. The slope of the curves refers to the sensitivity. The analyzed frequencies were: a) 3406 Hz, b) 10772 Hz and c) 23208 Hz. Modeling was made assuming: water resistivity 27 Ωm; sediment resistivity from 13.5 to 532 Ωm; water depth from 1 to 3m; inter-coil distance 1.66 m; sensor height above the water 0.7 m.

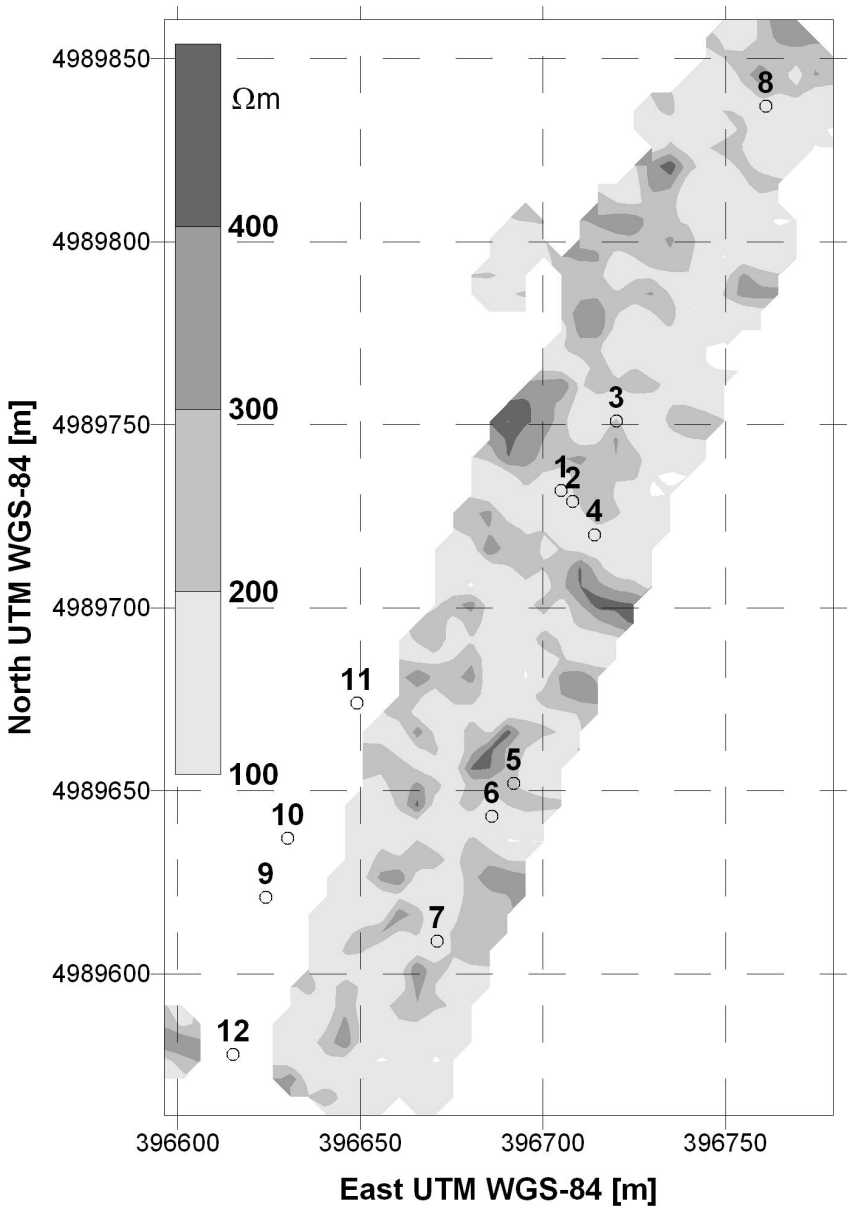

Figure 8 □ Resistivity map at 3925 Hz, after bathymetry correction. The circles (1-12) refer to the river bottom sampling points. Only points with a water depth of less than 2.5 m were considered.

Figure 9 ☐ Example of coarse riverbed sampled material.

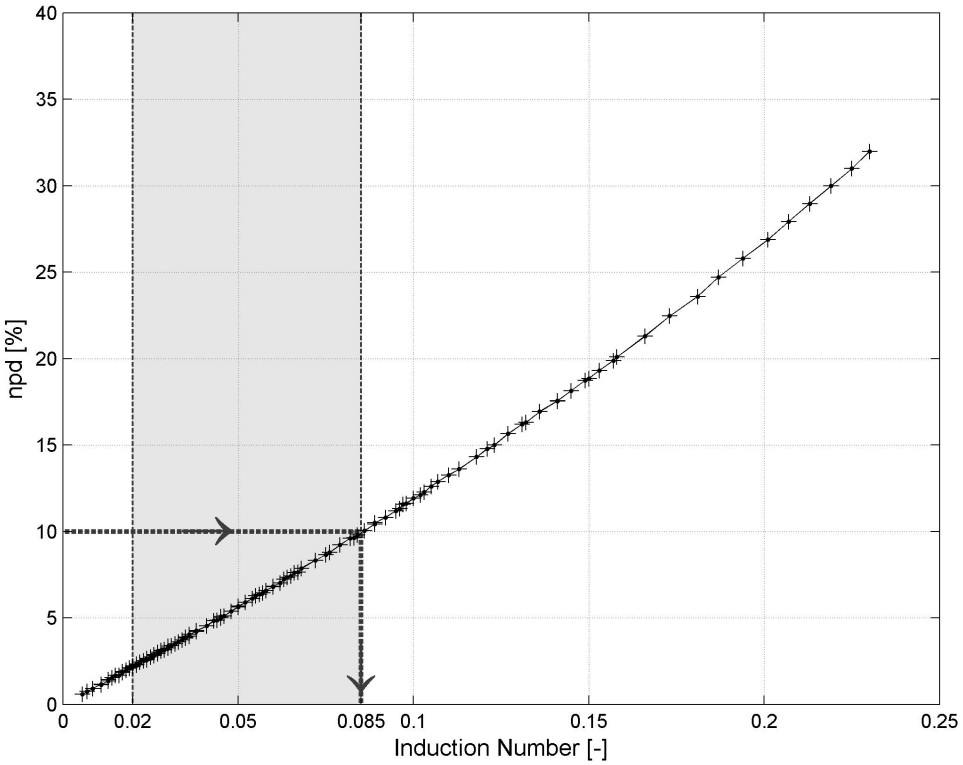

Figure A-1: Graph relating the normalized per-cent difference (npd) between the simplified form and the complete form of the quadrature component. The dashed band represents the B value range (0.02 < B < 0.085) that was considered. The upper B limit was obtained, as indicated by the black arrows, considering the largest acceptable npd equal to 10%.

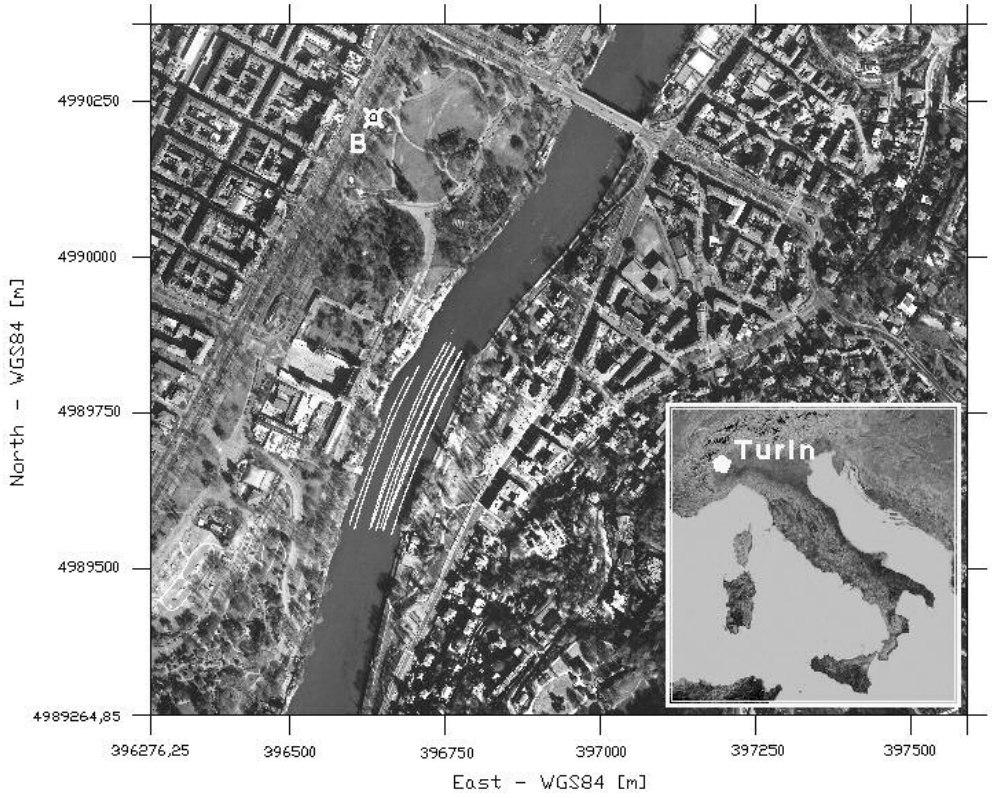

Figure 1 □ Localization of the investigated area with the survey tracks: the white lines indicate the continuous measurements (GEM-2 and GPR); the white cross in the NW corner of the map indicates the borehole (B) location.

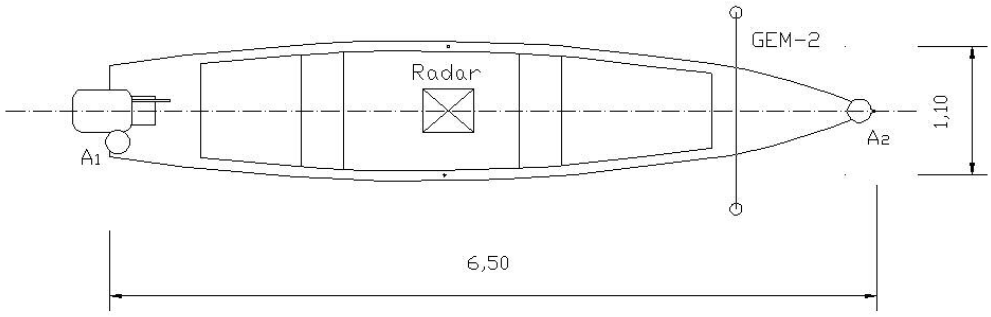

Figure 2 □ Layout of the motorboat used for the survey: A1 and A2 are the DGPS antennas; the dimensions are in meters.

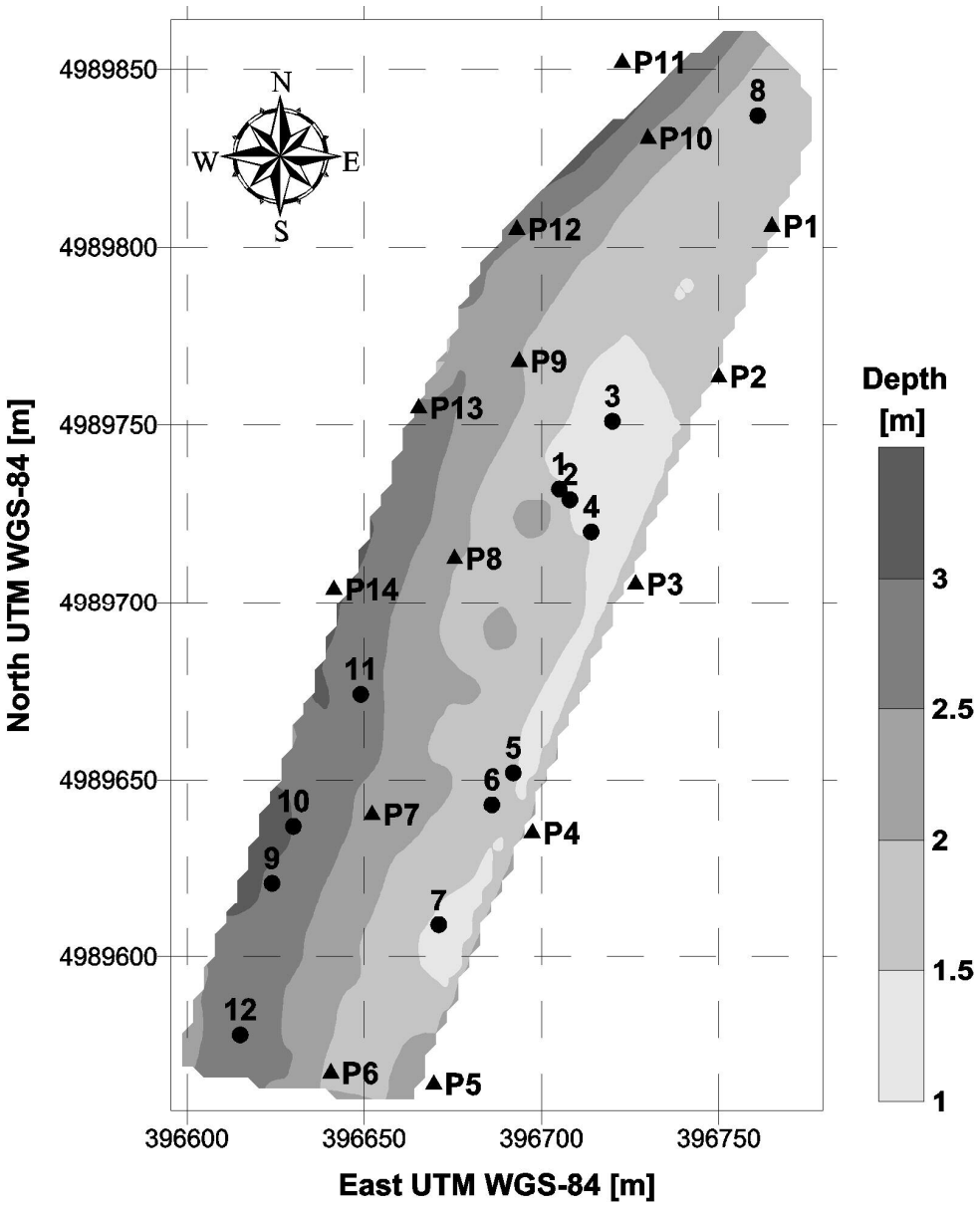

Figure 3 - Bathymetric map derived from GPR data: the triangles (P1-P14) refer to the water conductivity and permittivity sampling points; the circles (1-12) refer to river bottom sampling points.

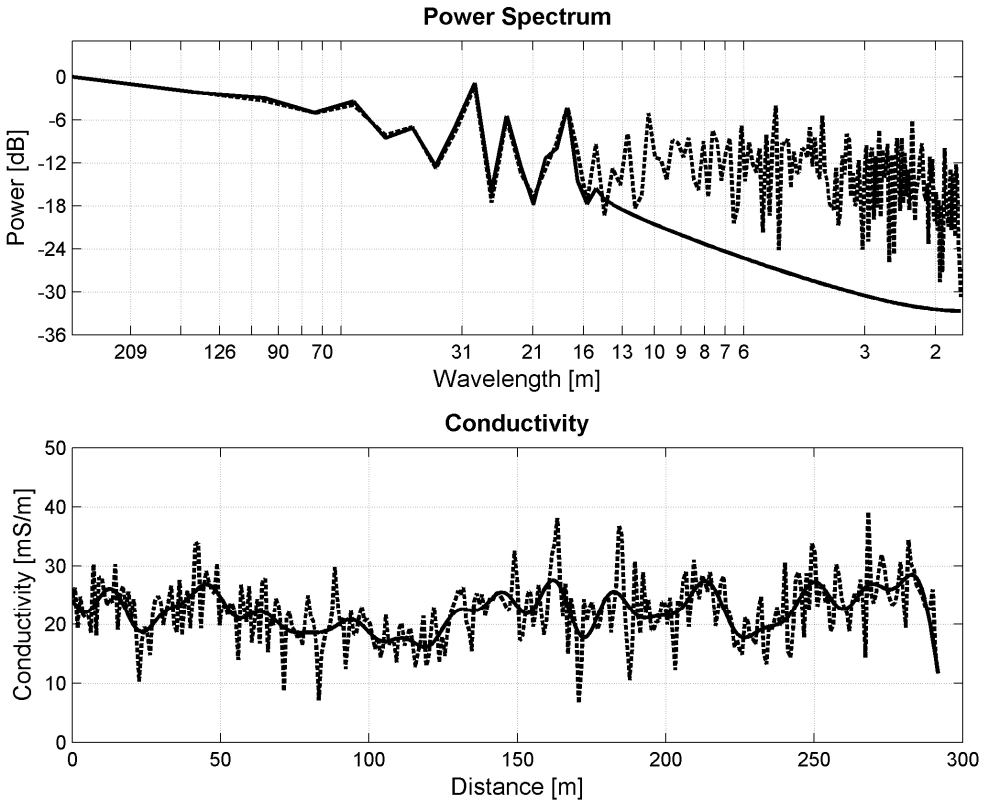

Figure 4 - Power spectrum (above) and conductivity profile (below). Comparison between raw (dashed line) and filtered (continuous line) data for track 3 at 3925 Hz (the third track from the West bank).

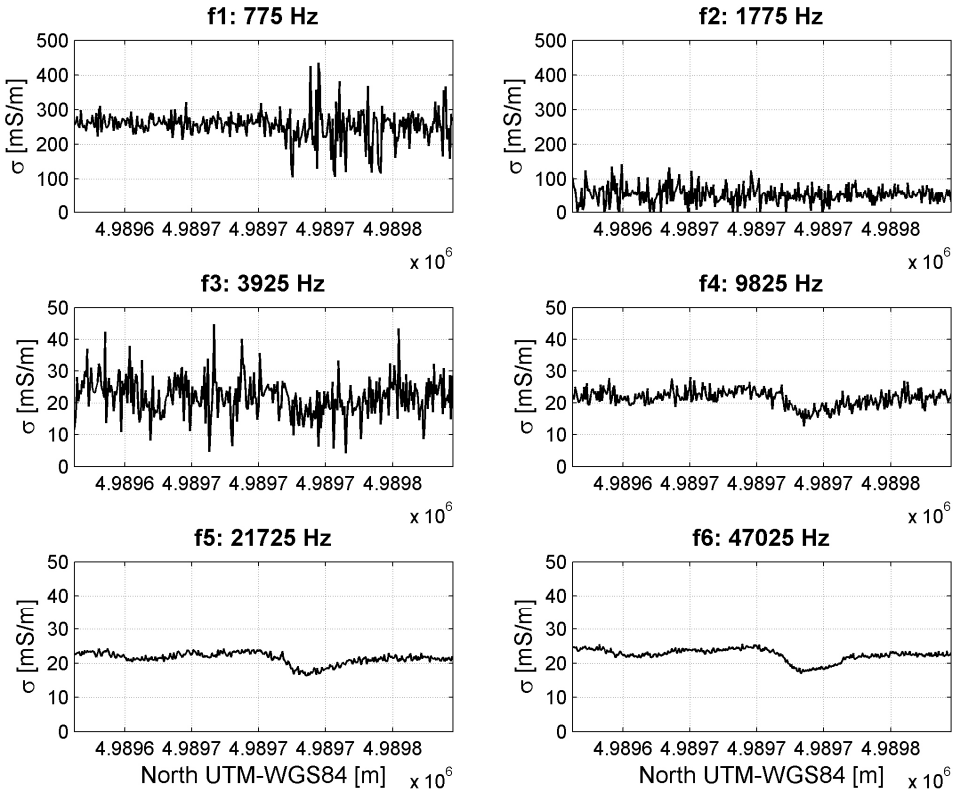

Figure 5 □ Raw conductivity profiles relative to all frequencies along track 3.

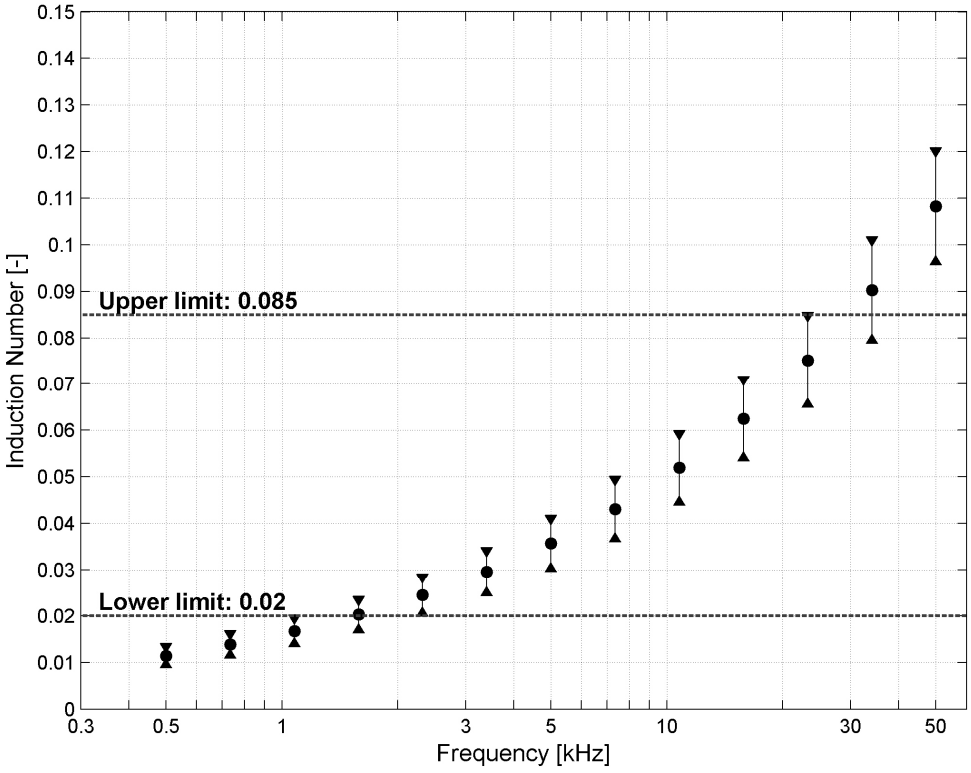

Figure 6 - Mean and standard deviation plot graph of the induction numbers estimated from the modeling in the 500-50000 Hz frequency range. Modeling was made assuming: water resistivity 27 Ωm; sediment resistivity from 13.5 to 532 Ωm; water depth from 1 to 3m; inter-coil distance 1.66 m; sensor height above the water 0.7 m.

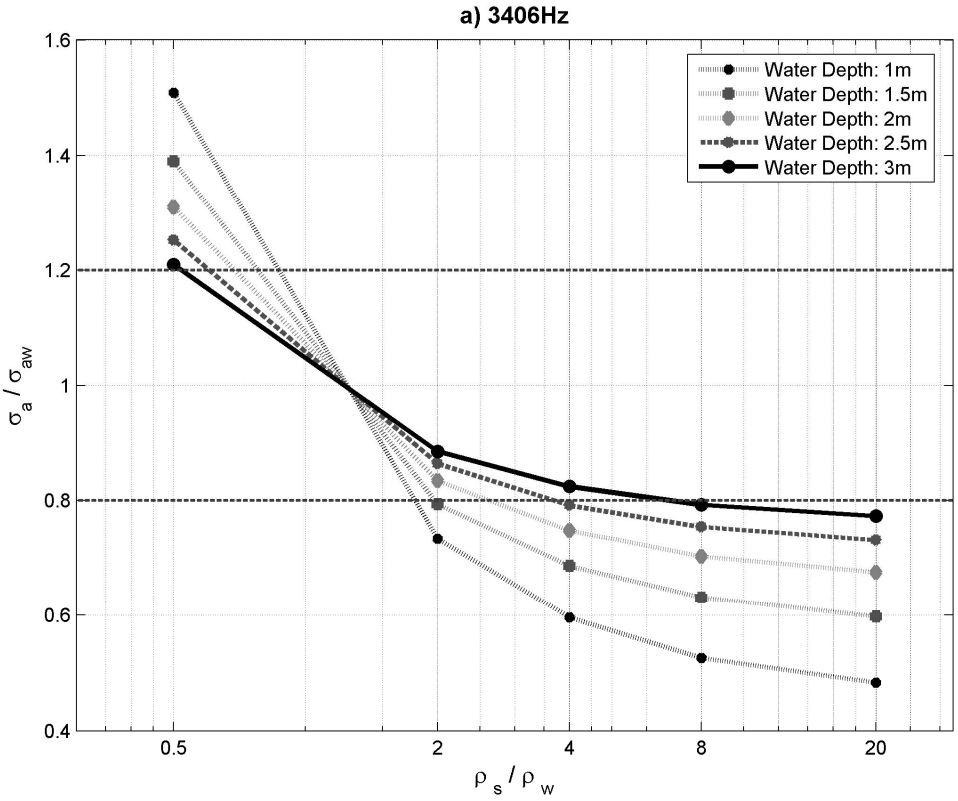

Figure 7 □ Synthetic apparent conductivity curves (normalized to the apparent conductivity of a water half-space) as a function of sediment resistivity (normalized to water resistivity). The horizontal dashed lines at 0.8 and 1.2 are the DOI thresholds. The parts of the curves outside this interval indicate detectable sediment resistivities. The slope of the curves refers to the sensitivity. The analyzed frequencies were: a) 3406 Hz, b) 10772 Hz and c) 23208 Hz. Modeling was made assuming: water resistivity 27 Ωm; sediment resistivity from 13.5 to 532 Ωm; water depth from 1 to 3m; inter-coil distance 1.66 m; sensor height above the water 0.7 m.

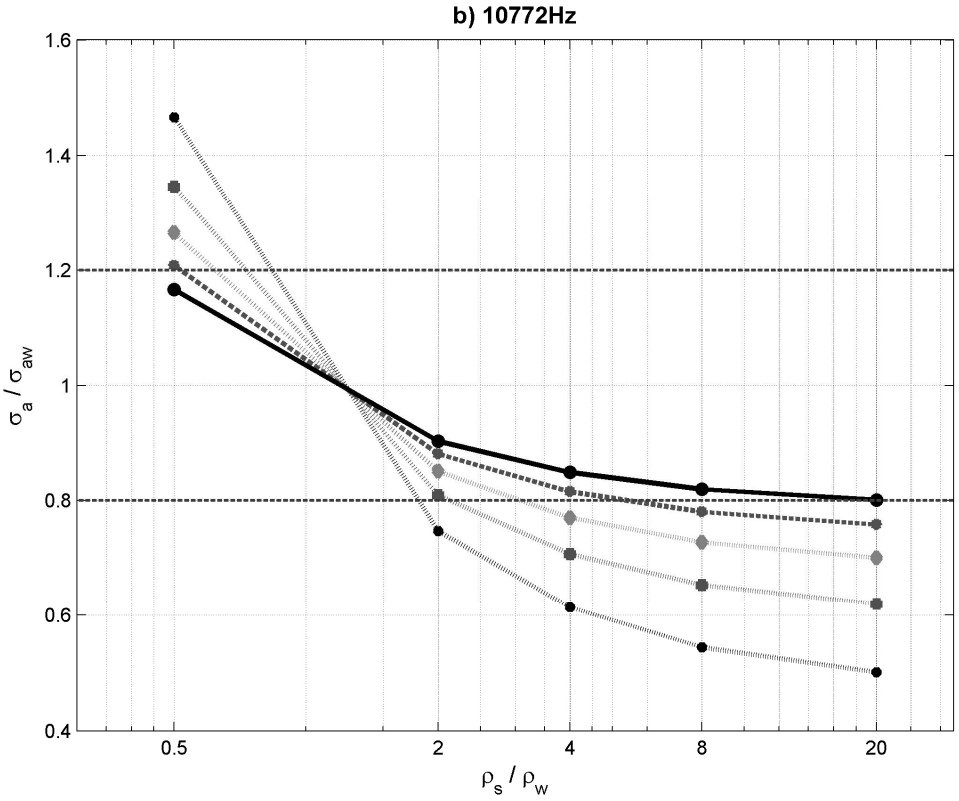

Figure 7 □ Synthetic apparent conductivity curves (normalized to the apparent conductivity of a water half-space) as a function of sediment resistivity (normalized to water resistivity). The horizontal dashed lines at 0.8 and 1.2 are the DOI thresholds. The parts of the curves outside this interval indicate detectable sediment resistivities. The slope of the curves refers to the sensitivity. The analyzed frequencies were: a) 3406 Hz, b) 10772 Hz and c) 23208 Hz. Modeling was made assuming: water resistivity 27 Ωm; sediment resistivity from 13.5 to 532 Ωm; water depth from 1 to 3m; inter-coil distance 1.66 m; sensor height above the water 0.7 m.

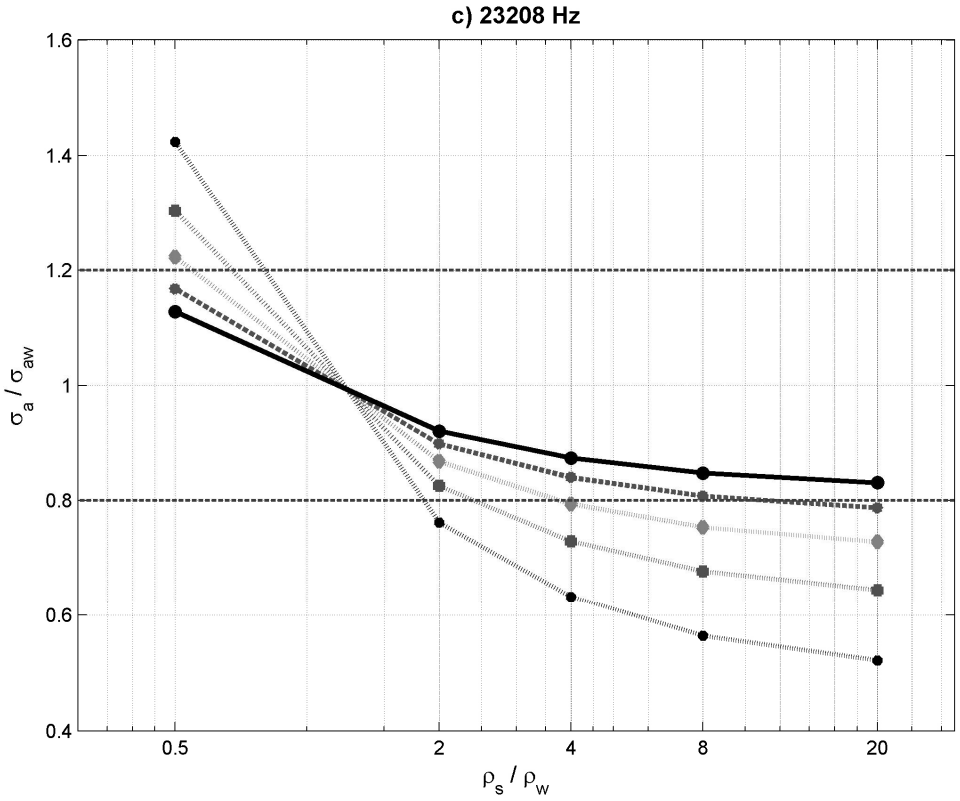

Figure 7 □ Synthetic apparent conductivity curves (normalized to the apparent conductivity of a water half-space) as a function of sediment resistivity (normalized to water resistivity). The horizontal dashed lines at 0.8 and 1.2 are the DOI thresholds. The parts of the curves outside this interval indicate detectable sediment resistivities. The slope of the curves refers to the sensitivity. The analyzed frequencies were: a) 3406 Hz, b) 10772 Hz and c) 23208 Hz. Modeling was made assuming: water resistivity 27 Ωm; sediment resistivity from 13.5 to 532 Ωm; water depth from 1 to 3m; inter-coil distance 1.66 m; sensor height above the water 0.7 m.

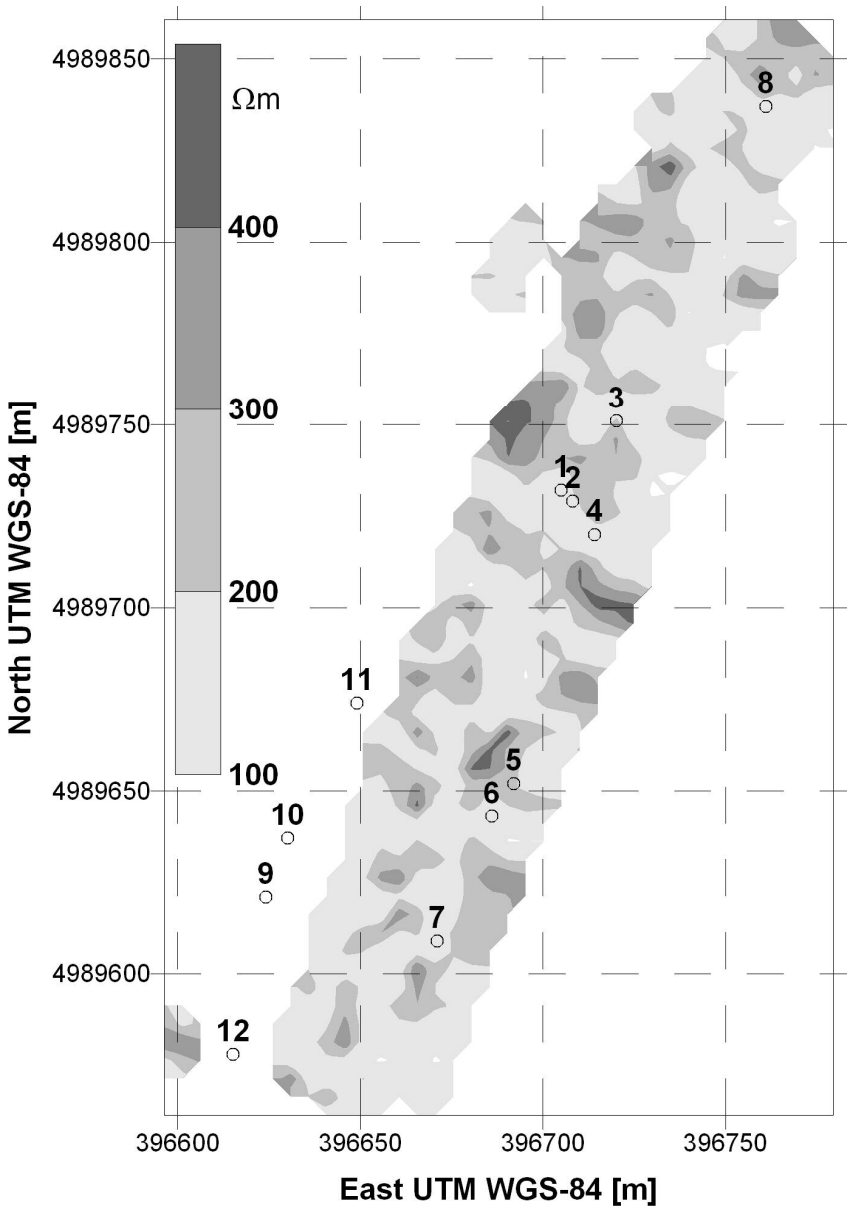

Figure 8 □ Resistivity map at 3925 Hz, after bathymetry correction. The circles (1-12) refer to the river bottom sampling points. Only points with a water depth of less than 2.5 m were considered.

Figure 9 □ Example of coarse riverbed sampled material.

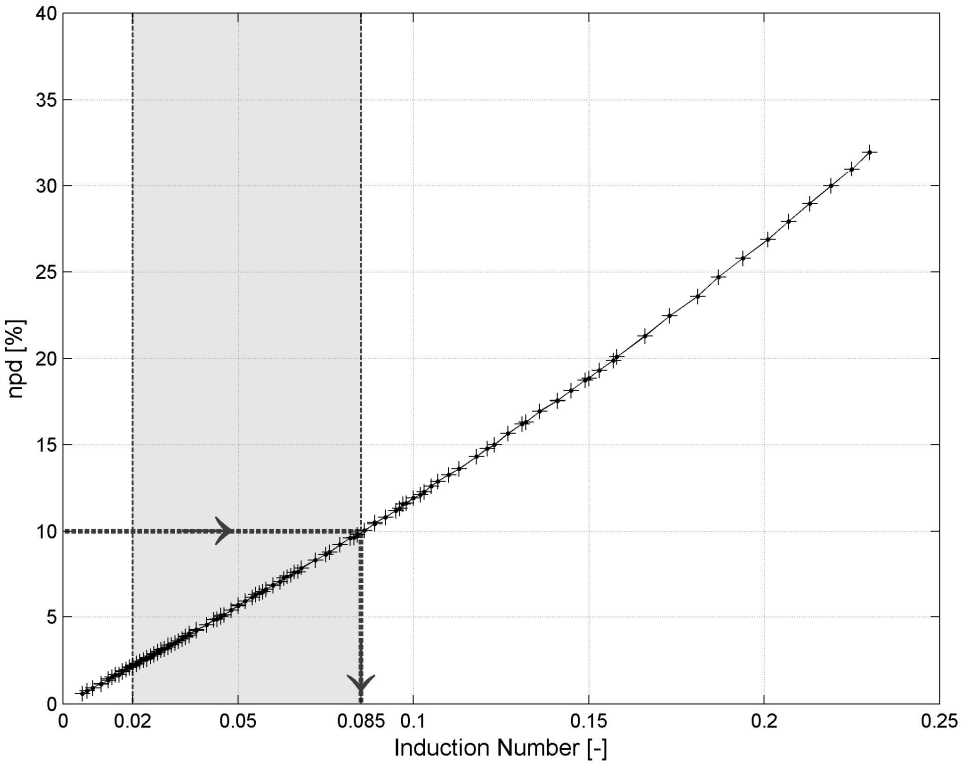

Figure A-1: Graph relating the normalized per-cent difference (npd) between the simplified form and the complete form of the quadrature component. The dashed band represents the B value range (0.02 < B < 0.085) that was considered. The upper B limit was obtained, as indicated by the black arrows, considering the largest acceptable npd equal to 10%.

MS #: 2006-0287.R2

Manuscript Type: Case History

Title: Study of riverine deposits using electromagnetic methods at low induction number

RRH: Riverine deposits mapping by broadband EM

Authors: Luigi Sambuelli[1], Salvatore Leggieri[1], Corrado Calzoni[1], Chiara Porporato[1]

[1]Politecnico di Torino, DITAG, Dipartimento di Ingegneria del Territorio, dell'Ambiente e delle Geotecnologie, Turin, Italy. E-mail: luigi.sambuelli@polito.it; todi.leggieri@libero.it; corrado.calzoni@polito.it; chiara.porporato@polito.it.